Unsteady aerodynamic models for agile flight at low Reynolds numbers

Steven L. Brunton*, Clarence W. Rowley†
Princeton University, Princeton, NJ 08544

The goal of this work is to develop low-order models for the unsteady aerodynamic forces on a small wing in response to agile maneuvers and gusts. In a previous study, it was shown that Theodorsen's and Wagner's unsteady aerodynamic models agree with force data from DNS for pitching and plunging maneuvers of a 2D flat plate at Reynolds numbers between 100 and 300 as long as the reduced frequency k is not too large, $k < 2$, and the effective angle-of-attack is below the critical angle. In this study reduced order models are obtained using an improved method, the eigensystem realization algorithm (ERA), which is more efficient to compute and fits within a standard control design framework. For test cases involving pitching and plunging motions, it is shown that Wagner's indicial response is closely approximated by ERA models of orders 4 and 6, respectively. All models are tested in a framework that decouples the longitudinal flight dynamic and aerodynamic models, so that the aerodynamics are viewed as an input-output system between wing kinematics and the forces generated. Lagrangian coherent structures are used to visualize the unsteady separated flow.

I. Introduction

A. Overview

The unsteady flow over small-scale wings has gained significant attention recently, both to study bird and insect flight as well as to develop advanced aerodynamic models for high-performance micro-aerial vehicles (MAVs). The short time scales involved in gusts and agile maneuvering make small wings susceptible to unsteady laminar separation, which can either enhance or destroy the lift depending on the specific maneuver. For example, certain insects[1–3] and birds[4] use the shape and motion of their wings to maintain the high transient lift associated with a rapid pitch-up, while avoiding stall and the substantially decreased lift which follows. The potential performance gains observed in bio-locomotion make this an interesting problem for model-based control in the arena of MAVs[5]. For a good overview of the effect of Reynolds number and aspect ratio on small wings, see Ol *et al.*[6,7].

Most aerodynamic models used for flight control rely on the quasi-steady assumption that lift and drag forces depend on parameters such as relative velocity and angle-of-attack in a static manner. The unsteady models of Theodorsen[8] and Wagner[9] are also widely used. Despite the wide variety of extensions and uses for these theories[10], they rely on a number of limiting idealizations, such as infinitesimal motions in an inviscid fluid, and an idealized planar wake, that result in linear models. These models do not describe the unsteady laminar separation characteristic of flows over small, agile wings. During gusts and rapid maneuvers, a small wing will experience high effective angle-of-attack which can result in unsteady separation. Dynamic stall occurs when the effective angle-of-attack changes rapidly so that a leading-edge vortex forms, provides temporarily enhanced lift and decreased pitching moment, and then sheds downstream, resulting in stall.[12]. This phenomenon is well known in the rotorcraft community[10] since it is necessary to pitch the blades down as they advance and pitch up as they retreat to balance lift in forward flight. Recently, there have been efforts to model the effect of dynamic stall on lift[13,14] as well as the lift coefficient due to post-stall vortex shedding[15].

*Graduate Student, Mechanical and Aerospace Engineering, Student Member, AIAA.
†Associate Professor, Mechanical and Aerospace Engineering, Associate Fellow, AIAA.

The goal of this study is to extend the range of unsteady aerodynamic models in a framework suitable for flight control, shown in Figure 1. In particular, the aerodynamics will be viewed as an input-output system with flight kinematic variables as inputs and aerodynamic forces as outputs. This framework has been specifically chosen to provide insights into how nonlinear dynamics in the aerodynamic model result in new bifurcations in the coupled flight model. Moreover, this approach most closely matches the DNS framework, which regards wing kinematics as inputs and provides force data as output.

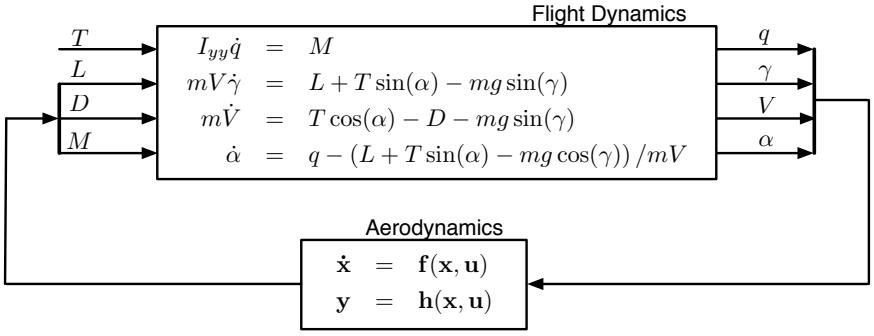

Figure 1. Schematic of the natural decoupling of flight dynamic and aerodynamic models. The modularity of this approach allows different aerodynamic models ranging from thin airfoil to Wagner's and Theodorsen's to ERA models can be plugged in with a common interface.

The remainder of the Introduction summarizes two previous studies. The first study [15] develops a heuristic model for the lift coefficient of an impulsively started flat plate at high angle-of-attack which includes a supercritical Hopf bifurcation to capture the unsteady laminar vortex shedding. The second study [16] compares classical unsteady aerodynamic models with DNS to determine for what flow conditions the model assumptions break down.

B. Enhanced Models for Separated Flow

A simple heuristic model which describes the transient and steady-state lift associated with an impulsively started 2D plate at a fixed angle-of-attack includes a Hopf bifurcation [15,18] in α and a decoupled first-order lag

$$\left.\begin{aligned} \dot{x} &= (\alpha - \alpha_c)\mu x - \omega y - ax(x^2 + y^2) \\ \dot{y} &= (\alpha - \alpha_c)\mu y + \omega x - ay(x^2 + y^2) \\ \dot{z} &= -\lambda z \end{aligned}\right\} \quad \Longrightarrow \quad \begin{aligned} \dot{r} &= r\left[(\alpha - \alpha_c)\mu - ar^2\right] \\ \dot{\theta} &= \omega \\ \dot{z} &= -\lambda z \end{aligned} \tag{1}$$

The z direction is decoupled and represents the exponential decay of transient lift generated from the impulsive start. The fixed point at $r = 0$ undergoes a supercritical Hopf bifurcation at $\alpha = \alpha_c$ resulting in an unstable fixed point at $r = 0$ and a stable limit cycle with radius $R = \sqrt{(\alpha - \alpha_c)\mu/a}$. The limit cycle represents fluctuations in lift due to periodic vortex shedding of a plate at an angle-of-attack which is larger than the angle at which the separation bubble bursts. Thus, at a particular angle-of-attack α, the unsteady coefficient of lift C_L is constructed from the average lift $\bar{C}_L$ and the state variables y and z as follows

$$C_L = \bar{C}_L + y + z$$

Proper orthogonal decomposition and Galerkin projection have also been shown to produce modes and models which preserve Lagrangian coherent structures [16]. In both models, the unsteady vortex shedding around a fixed plate at $Re = 100$ and $\alpha = 30^\circ$ is well characterized by a 2-mode model. However, there are fundamental limitations to these models such as the need to precisely tune model (1) and the limited range of angle-of-attack and Reynolds number. It is also unclear how to incorporate external forcing into the model $\dot{\mathbf{x}} = \ldots + \mathbf{f}(\alpha, \dot{\alpha})$, so that the terms $\mathbf{f}$ can excite the states $\mathbf{x}$ through a change of angle-of-attack or center-of-mass motion. This is the subject of current research.

C. Breakdown of Classical Models at High Angle-of-Attack

When modeling the aerodynamic forces acting on an airfoil in motion, it is natural to start with a quasi-steady approximation. Thin airfoil theory assumes that the airfoil's vertical center-of-mass, y, and angle-of-attack, α, motion is relatively slow so the flow field locally equilibrates to the motion. Thus, $\dot{y}$ and $\dot{\alpha}$ effects may be explained by effective angle-of-attack and effective camber, respectively.

$$C_L = 2\pi\left(\alpha + \dot{y} + \frac{1}{2}\dot{\alpha}\left(\frac{1}{2} - a\right)\right) \tag{2}$$

Lengths are nondimensionalized by $2b$ and time is nondimensionalized by $2b/U_\infty$, where U_∞ is the free stream velocity, b is the half-chord length and a is the pitch axis location with respect to the 1/2-chord (e.g., pitching about the leading edge corresponds to $a = -1$, whereas the trailing edge is $a = 1$).

Theodorsen's frequency domain model includes additional terms to account for the mass of air immediately displaced (apparent mass), and the circulatory lift from thin airfoil theory is multiplied by Theodorsen's transfer function $C(k)$ relating sinusoidal inputs of reduced frequency[17] k to their aerodynamic response.

$$C_L = \underbrace{\frac{\pi}{2}\left[\ddot{y} + \dot{\alpha} - \frac{a}{2}\ddot{\alpha}\right]}_{\text{Added-Mass}} + \underbrace{2\pi\left[\alpha + \dot{y} + \frac{1}{2}\dot{\alpha}\left(\frac{1}{2} - a\right)\right]C(k)}_{\text{Circulatory}} \tag{3}$$

Using Wagner's time domain method[9] it is possible to reconstruct the lift response to arbitrary input $u(t)$ using Duhamel superposition of the "indicial" lift response $C_L^\delta(t)$ due to a step-response in input, $\dot{u} = \delta(t)$.

$$C_L^{\alpha(t)}(t) = C_L^\delta(t)u(0) + \int_0^t C_L^\delta(t-\tau)\dot{u}(\tau)d\tau \tag{4}$$

In a previous study[16], thin airfoil theory, Theodorsen's model, and Wagner's indicial response were compared with forces obtained from DNS for pitching and heaving airfoils. Theodorsen's model showed agreement for moderate reduced frequencies $k < 2.0$ for a range of Strouhal numbers for which the maximum effective angle-of-attack is smaller than the critical stall angle. However, none of the models agreed with DNS when the actual or effective angle-of-attack exceeded the critical stall angle, which is a fundamental limitation of each method.

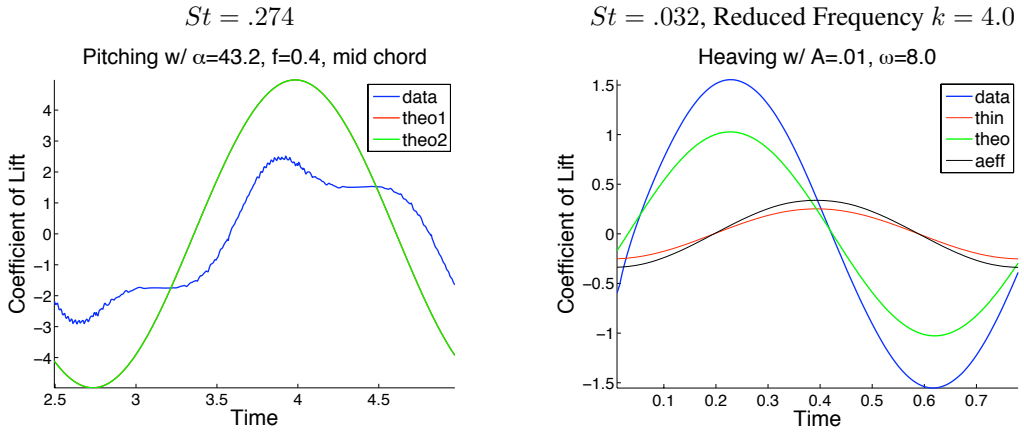

Figure 2. Each curve is a plot of lift coefficient vs. time for a sinusoidally pitching (left) or plunging (right) flat plate at Re $= 100$. The blue curve is the C_L from DNS, the red curve is computed using thin airfoil theory, Eq. (2), the black curve uses an effective angle-of-attack approximation, and the green curve is Theodorsen's prediction, Eq. (3). Theodorsen's model does not agree with DNS for reduced frequencies $k > 2.0$ or for Strouhal numbers exceeding $.256$, corresponding to large maximum effective angle-of-attack.

II. Methods

A. Immersed boundary method

Using a fully resolved direct numerical simulation based on an immersed boundary method developed by Taira and Colonius [19,20], it is possible to construct incompressible flow experiments at low Reynolds numbers and obtain velocity snapshots of the flow field. Here, we describe the results time resolved 2D simulations performed at a Reynolds number range of 100-300. The velocity field is defined on five nested grids; the finest grid covers a 4×4 domain and the coarsest grid covers a 64×64 domain, non-dimensionalized by chord length. Each grid has resolution 400×400. In a previous study [15], the steady-state lift of a flat plate was computed for angle-of-attack $\alpha \in [0, 90]$, exhibiting a Hopf bifurcation in lift at $\alpha_c \approx 28°$. For $\alpha > \alpha_c$, a stable limit cycle develops, corresponding to periodic vortex shedding from the leading and trailing edge.

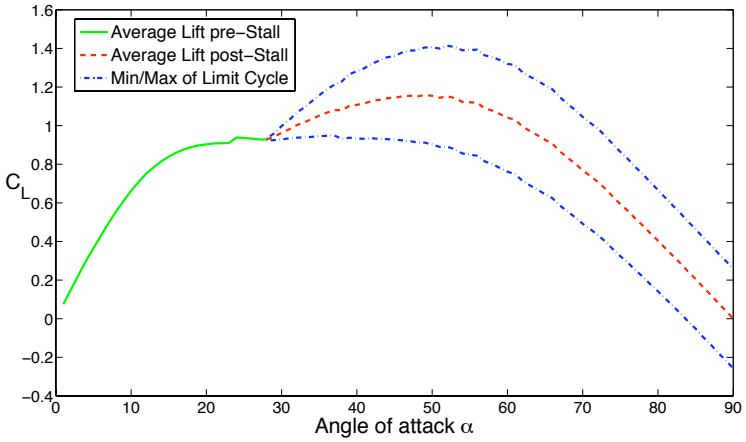

Figure 3. Lift vs. angle-of-attack for fixed plate at $Re = 100$. Hopf bifurcation occurs at $\alpha \approx 28°$. Dashed line represents average post-stall lift and dotted lines represent minimum and maximum post-stall lift.

B. Finite Time Lyapunov Exponents

To characterize the unsteady fluid dynamics of airfoils at low Reynolds numbers, it is important to identify regions of separated flow as well as wake structures. For an unsteady flow field, it is not possible to identify separated regions with streamlines alone [21]. Lagrangian coherent structures [22–25] (LCS), which are computed from a time-resolved sequence of snapshots of an unsteady flow, indicate regions of large stretching between nearby particles as ridges in the field of finite time Lyapunov exponents (FTLE) that satisfy an additional hyperbolicity condition [21]. FTLE fields may be computed using backward (resp. forward) time integration of particle grids, in which case the LCS represents attracting (resp. repelling) material lines and isolate regions of separated flow around the plate and sluggish flow in the wake. In the following visualizations, FTLE fields measuring stretching in backward time are used to obtain structures that attract particles in forward time. FTLE fields for four interesting cases are shown in Figure 4, where ridges, plotted in blue, indicate the boundaries of a separation bubble. For the case of a stationary plate at $\alpha = 25°$, the ridges coincide with streamlines outlining the separation bubble, since the flow field is steady; however, for each of the other three unsteady cases, the FTLE ridges are not the same as streamlines.

C. Eigensystem Realization Algorithm (ERA)

The Eigensystem Realization Algorithm (ERA) [27] is a method of obtaining reduced order models for high dimensional linear dynamical systems. It has recently been shown that ERA provides the same reduced order models as the method of snapshot-based balanced proper orthogonal decomposition (BPOD), more efficiently and without the need for adjoint simulations [26].

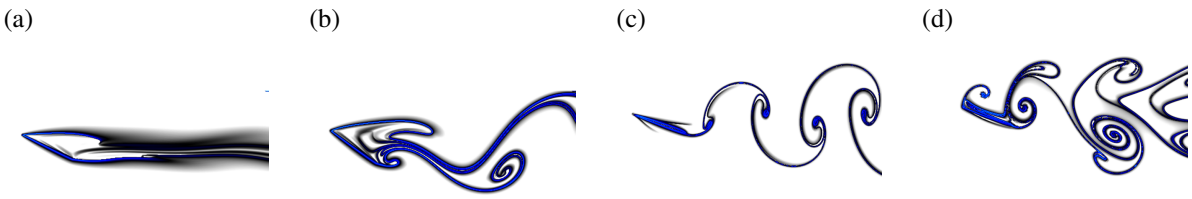

Figure 4. Lagrangian coherent structures for a variety of stationary and moving plates. (a) Stationary plate at $\alpha = 25^\circ$ (b) Stationary plate at $\alpha = 35^\circ$ (c) Pitching plate (d) Plunging plate with 20° bias. Ridges in the FTLE field are plotted in blue and represent the boundaries of a separation bubble. The flow field associated with a stationary plate at $\alpha = 25^\circ$ is the only steady case, and in thus FTLE ridges coincide with streamlines. In each of the other cases, FTLE ridges do not coincide with streamlines.

Consider a stable, discrete-time system with high dimensional state $\mathbf{x}(k) \in \mathbb{R}^n$ and multiple inputs $\mathbf{u}(k) \in \mathbb{R}^p$ and outputs $\mathbf{y}(k) \in \mathbb{R}^q$. The goal of reduced order modeling is to obtain a low dimensional system of order $r \ll n$ that preserves the input-output dynamics:

$$\left.\begin{aligned} \mathbf{x}(k+1) &= A\mathbf{x}(k) + B\mathbf{u}(k) \\ \mathbf{y}(k) &= C\mathbf{x}(k) \end{aligned}\right\} \xrightarrow{\text{Reduction}} \begin{aligned} \mathbf{x}_r(k+1) &= A_r\mathbf{x}_r(k) + B_r\mathbf{u}(k) \\ \mathbf{y}(k) &= C_r\mathbf{x}_r(k) \end{aligned} \tag{5}$$

ERA is a method of model reduction based on impulse-response simulations. Following[26] ERA consists of three steps:

1. Gather $(m_c+m_o)+2$ outputs from an impulse-response simulation, where m_c and m_o are integers representing the number of snapshots for controllability and observability. The outputs $\mathbf{y}(k) = CA^kB$ are called Markov parameters, and are synthesized into a generalized Hankel matrices:

$$H = \begin{bmatrix} CB & CAB & \cdots & CA^{m_c}B \\ CAB & CA^2B & \cdots & CA^{m_c+1}B \\ \vdots & \vdots & \ddots & \vdots \\ CA^{m_o}B & CA^{m_o+1}B & \cdots & CA^{m_c+m_o}B \end{bmatrix} \tag{6}$$

$$H' = \begin{bmatrix} CAB & CA^2B & \cdots & CA^{m_c+1}B \\ CA^2B & CA^3B & \cdots & CA^{m_c+2}B \\ \vdots & \vdots & \ddots & \vdots \\ CA^{m_o+1}B & CA^{m_o+2}B & \cdots & CA^{m_c+m_o+1}B \end{bmatrix} \tag{7}$$

2. Compute the singular value decomposition of H:

$$H = U\Sigma V^* = \begin{bmatrix} U_1 & U_2 \end{bmatrix} \begin{bmatrix} \Sigma_1 & 0 \\ 0 & 0 \end{bmatrix} \begin{bmatrix} V_1^* \\ V_2^* \end{bmatrix} = U_1\Sigma_1 V_1^* \tag{8}$$

3. Finally, let Σ_r be the first $r \times r$ block of Σ_1, U_r, V_r the first r columns of U_1, V_1, and the reduced order A_r, B_r, C_r are given as follows:

$$A_r = \Sigma_r^{-1/2} U_r^* H' V_r \Sigma_r^{-1/2} \tag{9}$$

$$B_r = \text{ first } p \text{ columns of } \Sigma_r^{1/2} V_1^* \tag{10}$$

$$C_r = \text{ first } q \text{ rows of } U_r \Sigma_r^{1/2} \tag{11}$$

III. Results

Using the immersed boundary method, step-responses are simulated for pitch-up and plunge-up maneuvers. The lift coefficient C_L is viewed as the output, and the inputs are either angle-of-attack α or vertical center-of-mass velocity $\dot{y}$. Applying the eigensystem realization algorithm (ERA) to the step-response data results in reduced order models which accurately reproduce the input-output behavior between the pitch and plunge inputs and the output C_L.

A. Impulsive-Response Data

In order to obtain reduced order models using ERA, it is necessary to obtain impulse-response data. Here, the two impulse-response experiments correspond to an step increase of 1° in angle-of-attack, $\dot{\alpha} = \delta(t)$, rotated about the mid-chord, and a step increase of .01 in plunging velocity, $\ddot{y} = .01 \cdot \delta(t)$. To numerically simulate a step-response in a given variable u, instead of setting $\dot{u} = \delta(t)$, it is convenient to set u equal to a sharp sigmoidal function. Figure 5 shows the step-response lift data (top), along with the sigmoid (bottom). The step-response in pitch angle is simulated with time-step .0001 and sigmoidal step duration .01, and the step-response in vertical velocity is simulated with time-step .001 and sigmoidal step duration .011; this yields step-responses which are resolved in time.

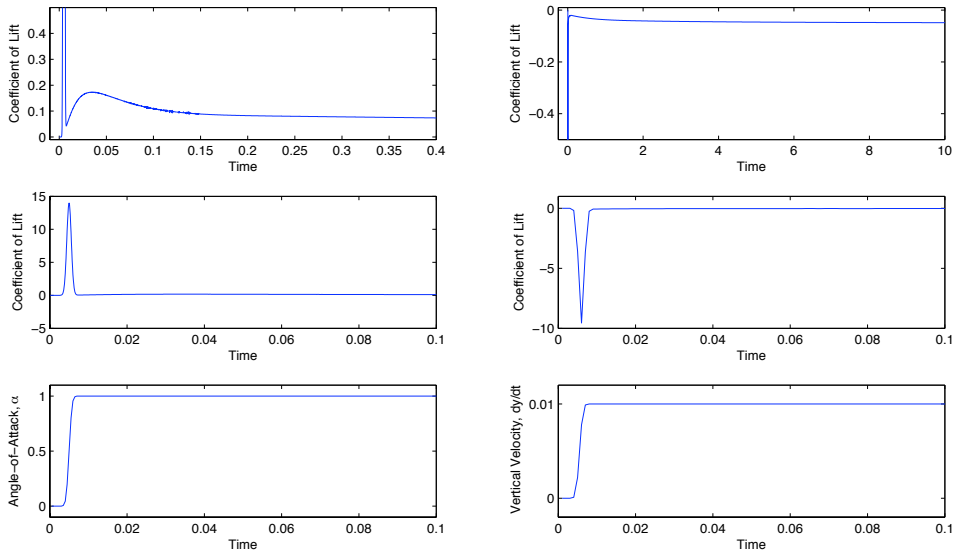

Figure 5. Lift coefficient vs. time for step-response at $Re = 300$. (Left) 1° pitch-up about mid-chord , (Right) plunge-up to $\dot{y} = .01$. (Top) Non-zero steady state lift for large times, (Middle & Bottom) Transient lift for short times.

In order to visualize the unsteady flow field associated with pitch-up and plunge-up maneuvers, it is helpful to use a sigmoid with a larger magnitude, spread out over a longer time. Figure 6 shows the lift coefficient plotted against time for exaggerated pitch-up and plunge maneuvers. Additionally, snapshots from DNS are shown in Figures 7 & 8.

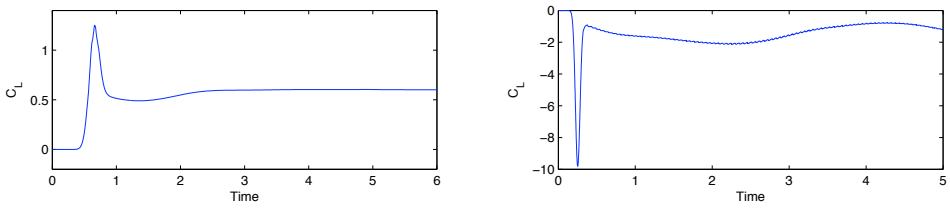

Figure 6. Lift coefficient vs. time for step-response at $Re = 300$. (Left) 8° pitch-up, (Right) plunge-up maneuver to $\dot{y} = .375$.

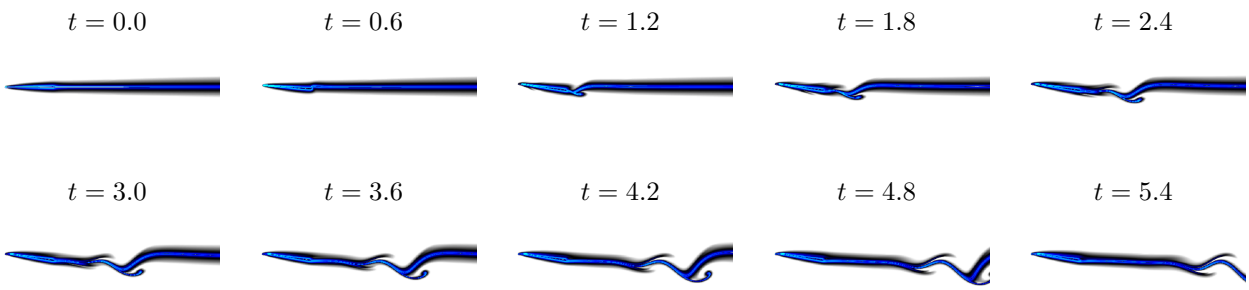

Figure 7. Snapshots for a sigmoidal pitch-up maneuver. Blue regions have large finite time Lyapunov exponent, illustrating the boundary layer, separated flow, and wake structures.

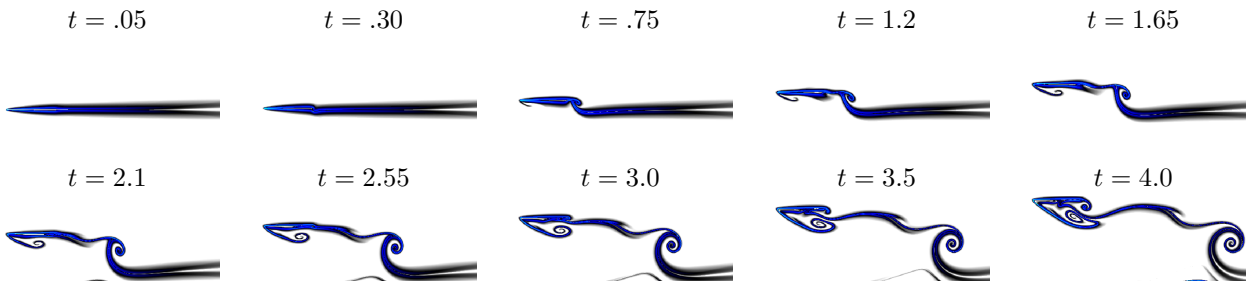

Figure 8. Snapshots for a sigmoidal plunge-up maneuver. Blue regions have large finite time Lyapunov exponent, illustrating the boundary layer, separated flow, and wake structures.

B. Model Comparison– Pitching Maneuvers

The step-response in pitch angle α is used to construct a $m_c \times m_o$ Hankel matrix with $m_c = m_o = 500$. A $4-$mode ERA model captures the step-response well, as shown in Figure 9.

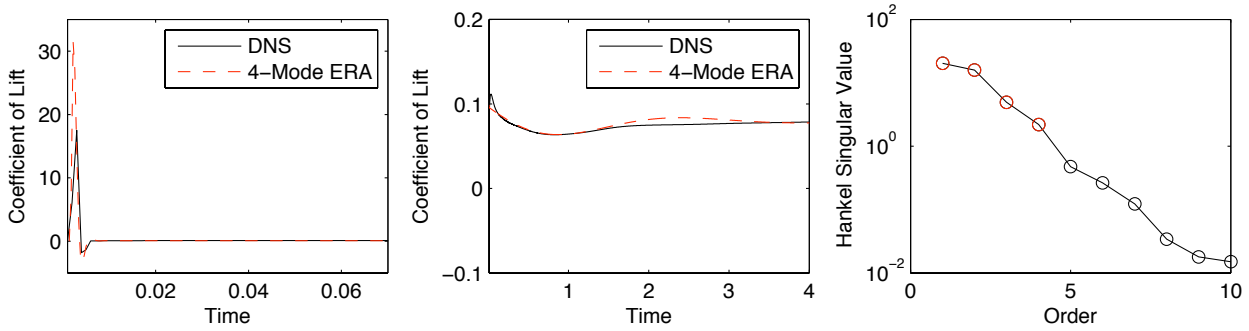

Figure 9. Step-response (left) and Hankel singular values (right) for 1° pitch-up. DNS (black) is compared with a 4-mode ERA model (red).

Figure 10 shows a comparison of the ERA model with direct numerical simulation (DNS) as well as Theodorsen's and Wagner's models for a number of pitching maneuvers. All pitching maneuvers are performed at the mid-chord to eliminate added-mass terms. Note the striking similarity between the ERA model and Wagner's indicial response.

This is to be expected, since as more modes are retained in a ERA model, the response should converge to Wagner's indicial response.

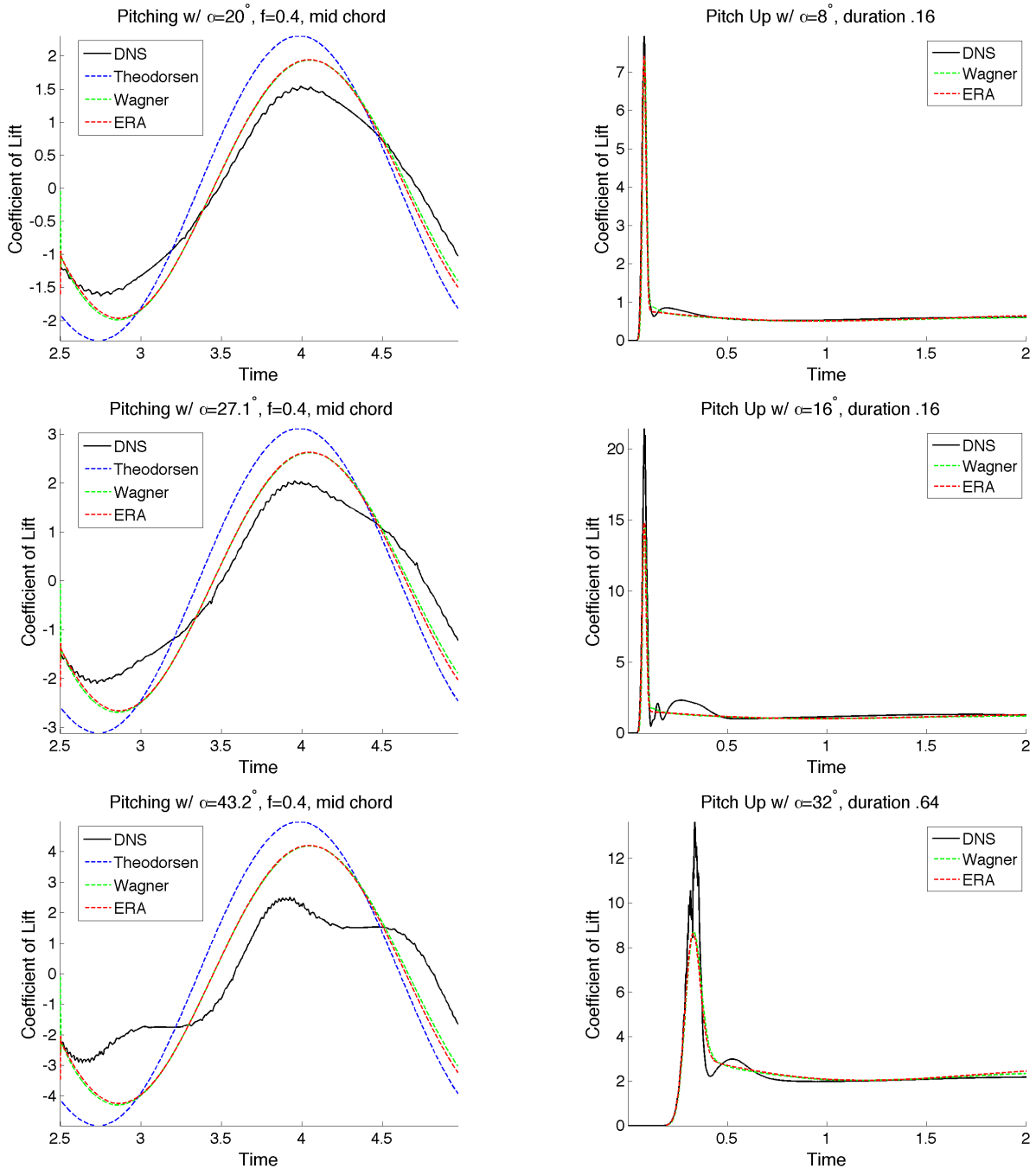

Figure 10. Comparison of lift models for sinusoidal pitching at $Re = 100$ (left) and impulse pitch-up maneuvers at $Re = 300$ (right).

The input to the ERA model is the time-derivative of the angle-of-attack, denoted $u_{\dot{\alpha}}$. Because the steady-state lift coefficient is nonzero for $\alpha(t) = 1°$, it is important to include a nonzero lift slope C_{L_α} in the model by augmenting the ERA state $\mathbf{x}$ with angle-of-attack α and including C_{L_α} in the C matrix as shown in Equation (12):

$$\frac{d}{dt}\begin{bmatrix}\mathbf{x}\\ \alpha\end{bmatrix} = \begin{bmatrix}A_{\text{ERA}} & 0\\ 0 & 0\end{bmatrix}\begin{bmatrix}\mathbf{x}\\ \alpha\end{bmatrix} + \begin{bmatrix}B_{\text{ERA}}\\ 1\end{bmatrix} u_{\dot{\alpha}}$$

$$C_L = \begin{bmatrix}C_{\text{ERA}} & C_{L_\alpha}\end{bmatrix}\begin{bmatrix}\mathbf{x}\\ \alpha\end{bmatrix} \tag{12}$$

$C_{L_\alpha} = .079$ is the steady state value of the step-response. $A_{\text{ERA}}, B_{\text{ERA}}, C_{\text{ERA}}, D_{\text{ERA}}$ are given in Appendix A.

C. Model Comparison– Plunging Maneuvers

The step-response in vertical velocity $\dot{y}$ is used to construct a $m_c \times m_o$ Hankel matrix with $m_c = m_o = 500$. A $6-$mode ERA model captures the impulse-response behavior, as shown in Figure 11.

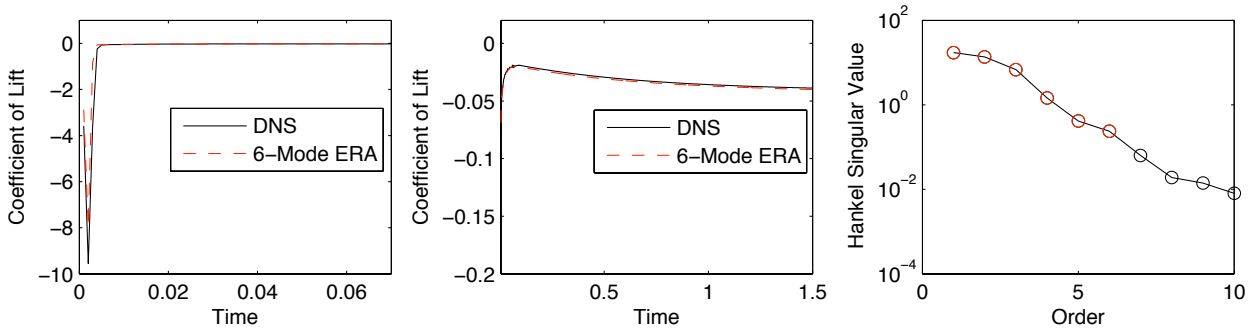

Figure 11. Step-response (left) and Hankel singular values (right) for plunge-up maneuver to $\dot{y} = .01$. DNS (black) is compared with an $6-$mode ERA model (red).

The input to the ERA model is the vertical acceleration of the plate, $u_{\ddot{y}}$. Because the steady-state lift coefficient is nonzero for $\dot{y}(t) \neq 0$, it is important to include the nonzero lift slope $C_{L_{\dot{y}}}$ in the model by augmenting the ERA state $\mathbf{x}$ with the plunging velocity $\dot{y}$ and including $C_{L_{\dot{y}}}$ in the C matrix:

$$\frac{d}{dt}\begin{bmatrix}\mathbf{x}\\ \dot{y}\end{bmatrix} = \begin{bmatrix}A_{\text{ERA}} & 0\\ 0 & 0\end{bmatrix}\begin{bmatrix}\mathbf{x}\\ \dot{y}\end{bmatrix} + \begin{bmatrix}B_{\text{ERA}}\\ 1\end{bmatrix} u_{\ddot{y}}$$

$$C_L = \begin{bmatrix}C_{\text{ERA}} & C_{L_{\dot{y}}}\end{bmatrix}\begin{bmatrix}\mathbf{x}\\ \dot{y}\end{bmatrix} \tag{13}$$

$C_{L_{\dot{y}}} = -4.56$ is determined from the steady-state value of the step-response.

Figure 12 shows a comparison of the ERA model with direct numerical simulation (DNS), Theodorsen's model and Wagner's model for several sinusoidally plunging plates with center-of-mass motion $y(t) = -A\sin(\omega t)$. Because the ERA model captures the step-response behavior, the close agreement with Wagner's indicial response is not surprising.

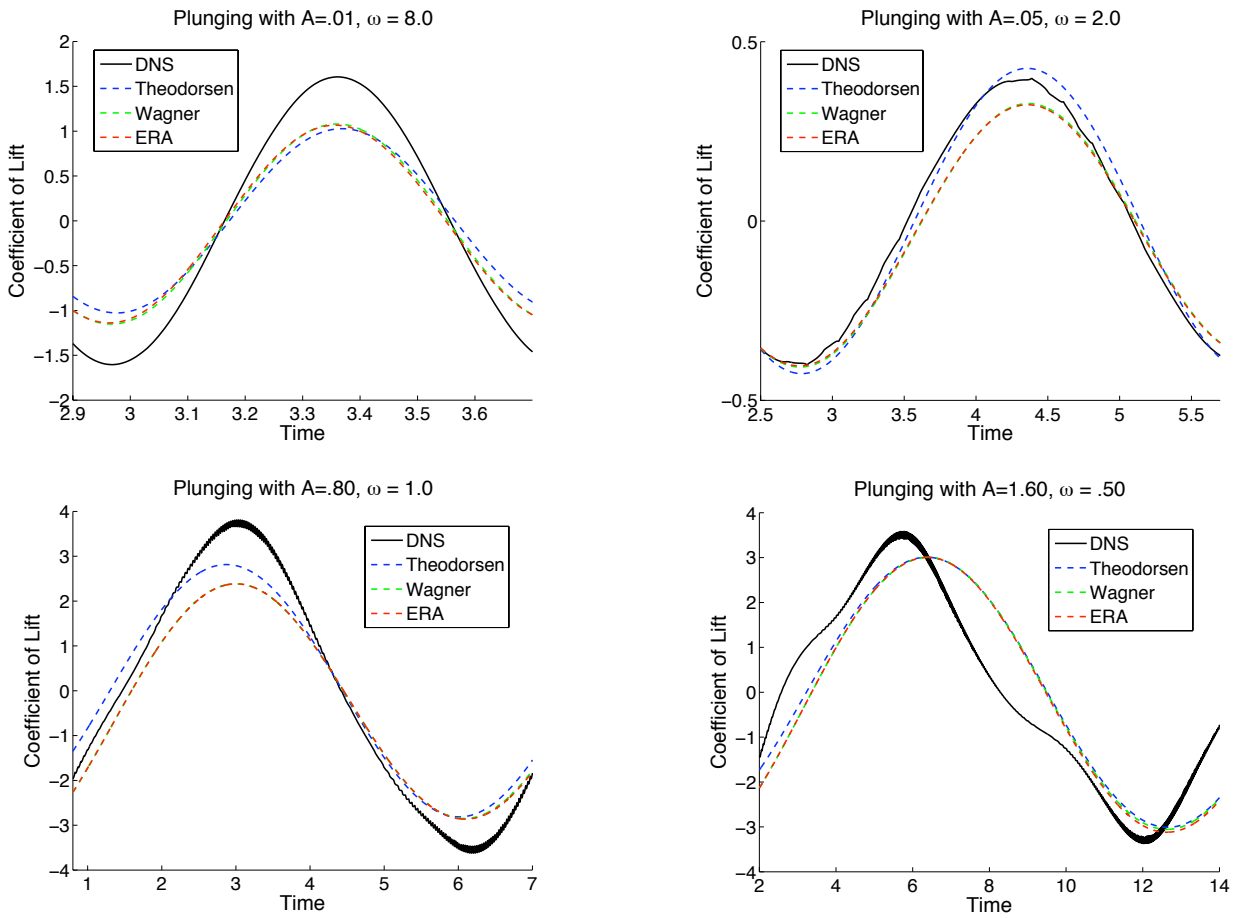

Figure 12. Comparison of DNS (black), Theodorsen's model (blue), Wagner's indicial response (green) and ERA (red) for sinusoidal plunging maneuver at $Re = 100$ with vertical motion $y(t) = -A\sin(\omega t)$.

IV. Conclusions

We have investigated the unsteady aerodynamic forces on low-Reynolds number wings in pitch and plunge maneuvers using 2D direct numerical simulations. The eigensystem realization algorithm (ERA) has been used to obtain reduced order models from step-response simulations in pitch angle α and vertical center-of-mass velocity $\dot{y}$. The ERA models for pitching and plunging plates yield an approximate lift coefficient that is strikingly similar to that obtained by Wagner's indicial response. This is to be expected since Wagner's method is based on the step response, which ERA approximates with a low order model.

Although the ERA models to not outperform Wagner or Theodorsen's models in reconstructing the lift force, they provide an important first step in developing a systematic framework for modeling and control. A low-order ERA model is significantly more efficient and tractable than Wagner's indicial response, which involves a convolution of the impulse-response with the control signal. Moreover, the ERA model fits naturally into the standard linear control theory framework and nicely decouples from the flight dynamic equations. Future work involves separating added-mass forces and viscous forces, and extending this framework to develop models for the viscous terms alone. Finally, augmenting the existing ERA models with nonlinear stall and separation models will be important for improved lift modeling.

Appendix A

ERA Pitching Model

$$A_{\text{ERA}} = \begin{bmatrix} -122.1 & 2022 & -38.02 & -6.645 \\ -2022 & -2322 & 62.73 & 100.6 \\ 38.02 & 62.73 & -1.716 & -4.151 \\ -6.645 & -100.6 & 4.151 & -.5052 \end{bmatrix} \tag{14}$$

$$B_{\text{ERA}} = \begin{bmatrix} 2.493 & 8.378 & -.2037 & .0885 \end{bmatrix}^T \tag{15}$$

$$C_{\text{ERA}} = \begin{bmatrix} 2.493 & -8.378 & .2037 & .0885 \end{bmatrix} \tag{16}$$

and $D_{\text{ERA}} = 0$. The eigenvalues of A_{ERA} are

$$\lambda_{1,2} = -1222 \pm 1699i \tag{17}$$
$$\lambda_{3,4} = -0.77 \pm 2.06i \tag{18}$$

ERA Plunging Model

$$A_{\text{ERA}} = \begin{bmatrix} -.099 & 6.962 & 1.433 & -43.7 & -.103 & .602 \\ -6.962 & -75.96 & -1143 & 658.1 & 6.084 & -23.5 \\ 1.433 & 1143 & -24.67 & 3694 & 2.183 & -14.77 \\ 43.7 & 658.1 & -3694 & -5815 & -68.14 & 234.5 \\ -.103 & -6.084 & 2.183 & 68.14 & -.297 & 3.52 \\ -.602 & -23.5 & 14.77 & 234.5 & -3.52 & -66.96 \end{bmatrix} \tag{19}$$

$$B_{\text{ERA}} = 100 \begin{bmatrix} .066 & 1.246 & -.6835 & -9.47 & .038 & .198 \end{bmatrix}^T \tag{20}$$

$$C_{\text{ERA}} = \begin{bmatrix} .066 & -1.246 & -.6835 & 9.47 & .038 & -.198 \end{bmatrix} \tag{21}$$

and $D_{\text{ERA}} = 0$. Here the B_{ERA} matrix is multiplied by $1/.01 = 100$ because the above model was calculated for a step-response in vertical velocity to $\dot{y} = .01$. The eigenvalues of A_{ERA} are

$$\lambda_{1,2} = -1995 \pm 1846i \tag{22}$$
$$\lambda_3 = -1935 \tag{23}$$
$$\lambda_4 = -56.8 \tag{24}$$
$$\lambda_5 = -1.9 \tag{25}$$
$$\lambda_6 = -0.3 \tag{26}$$

References

[1]Birch, J. and Dickinson, M., "Spanwise flow and the attachment of the leading-edge vortex on insect wings." *Nature*, Vol. 412, 2001, pp. 729–733.

[2]Sane, S., "The aerodynamics of insect flight." *J. Exp. Biol.*, Vol. 206, No. 23, 2003, pp. 4191–4208.

[3]Zbikowski, R., "On aerodynamic modelling of an insect-like flapping wing in hover for micro air vehicles," *Phil. Trans. R. Soc. Lond. A*, Vol. 360, 2002, pp. 273–290.

[4]Videler, J., Samhuis, E., and Povel, G., "Leading-edge vortex lifts swifts." *Science*, Vol. 306, 2004, pp. 1960–1962.

[5]Ahuja, S., Rowley, C., Kevrekidis, I., Wei, M., Colonius, T., and Tadmor, G., "Low-dimensional models for control of leading-edge vortices: Equilibria and linearized models." *AIAA Aerospace Sciences Meeting and Exhibit*, 2007.

[6]Ol, M., McAuliffe, B., Hanff, E., Scholz, U., and Kahler, C., "Comparison of laminar separation bubble measurements on a low Reynolds number airfoil in three facilities," *35th AIAA Fluid Dynamics Conference and Exhibit*, 2005.

[7]Kaplan, S., Altman, A., and Ol, M., "Wake vorticity measurements for low aspect ratio wings at low Reynolds number," *Journal of Aircraft*, Vol. 44, No. 1, 2007, pp. 241–251.

[8]Theodorsen, T., "General theory of aerodynamic instability and the mechanism of flutter," Tech. Rep. 496, NACA, 1935.

[9]Wagner, H., "Über die Entstehung des dynamischen Auftriebes von Tragflügeln," *Zeitschrift für Angewandte Mathematic und Mechanik*, Vol. 5, No. 1, 35 1925, pp. 17.

[10]Leishman, J. G., *Principles of Helicopter Aerodynamics*, Cambridge University Press, 2nd ed., 2006.

[11]Stengel, R., *Flight Dynamics*, Princeton University Press, 2004.

[12]Smith, A., *Vortex models for the control of stall.*, PhD thesis, Boston University, 2005.

[13]Magill, J., Bachmann, M., Rixon, G., and McManus, K., "Dynamic stall control using a model-based observer." *J. Aircraft*, Vol. 40, No. 2, 2003, pp. 355–362.

[14]Goman, M. and Khabrov, A., "State-space representation of aerodynamic characteristics of an aircraft at high angles of attack." *J. Aircraft*, Vol. 31, No. 5, 1994, pp. 1109–1115.

[15]Brunton, S., Rowley, C., Taira, K., Colonius, T., Collins, J., and Williams, D., "Unsteady aerodynamic forces on small-scale wings: experiments, simulations and models," *46th AIAA Aerospace Sciences Meeting and Exhibit*, 2008.

[16]Brunton, S. and Rowley, C., "Modeling the unsteady aerodynamic forces on small-scale wings," *47th AIAA Aerospace Sciences Meeting and Exhibit*, 2009.

[17]Koochesfahani, M. M., "Vortical patterns in the wake of an oscillating airfoil," *AIAA J.*, Vol. 27, 1989, pp. 1200–1205.

[18]Ahuja, S. and Rowley, C., "Low-dimensional models for feedback stabilization of unstable steady states," *AIAA Aerospace Sciences Meeting and Exhibit*, 2008.

[19]Taira, K. and Colonius, T., "The immersed boundary method: a projection approach." *J. Comput. Phys.*, Vol. 225, No. 2, 2007, pp. 2118–2137.

[20]Taira, K., Dickson, W., Colonius, T., Dickinson, M., and Rowley, C., "Unsteadiness in flow over a flat plate at angle-of-attack at low Reynolds numbers." *AIAA Aerospace Sciences Meeting and Exhibit*, 2007.

[21]Haller, G., "Lagrangian coherent structures from approximate velocity data," *Physics of Fluids*, Vol. 14, No. 6, 2002, pp. 1851–1861.

[22]Green, M., Rowley, C., and Haller, G., "Detection of Lagrangian coherent structures in 3D turbulence." *J. Fluid Mech.*, Vol. 572, 2007, pp. 111–120.

[23]Shadden, S., Lekien, F., and Marsden, J., "Definition and properties of Lagrangian coherent structures from finite-time Lyapunov exponents in two-dimensional aperiodic flows." *Physica D*, Vol. 212, No. 34, 2005, pp. 271–304.

[24]Lipinski, D., Cardwell, B., and Mohseni, K., "A Lagrangian analysis of two-dimensional airfoil with vortex shedding," *J. Phys. A: Math. Theor.*, Vol. 41, 2008.

[25]Holmes, P., Lumley, J., and Berkooz, G., *Turbulence, Coherent Structures, Dynamical Systems and Symmetry*, Cambridge University Press, 1996.

[26]Ma, Z., Ahuja, S., and Rowley, C., "Reduced order models for control of fluids using the Eigensystem Realization Algorithm," *Theor. Comput. Fluid. Dyn.*, 2009.

[27]Juang, J. and Pappa, R., "An eigensystem realization algorithm for modal parameter identification and model reduction," *J. Guid. Contr. dyn.*, Vol. 8, No. 5, 1985, pp. 620–627.

[28]Rowley, C., "Model reduction for fluids using balanced proper orthogonal decomposition." *Int. J. Bifurcation Chaos*, Vol. 15, No. 3, 2005, pp. 997–1013.